

Unraveling the role of dipolar vs. Dzyaloshinskii-Moriya interaction in stabilizing compact magnetic skyrmions

Anne Bernand-Mantel*

Cyrill B. Muratov†

Thilo M. Simon†

June 24, 2022

Abstract

Magnetic skyrmions have been the subject of extensive experimental studies in ferromagnetic thin films and multilayers, revealing a diversity in their size, stability and internal structure. While the orthodox skyrmion theory focuses on the Dzyaloshinskii-Moriya interaction (DMI) and neglects higher-order energy terms, it is becoming clear that the full stray field energy needs to be taken into account to understand these recent observations. Here we present a micromagnetic study based on rigorous mathematical analysis which allows to account for the full stray field energy in the thin film and low DMI regime. In this regime, the skyrmion profile is close to a Belavin-Polyakov profile, which yields analytical expressions for the equilibrium skyrmion radius and energy. The obtained formulas provide a clear identification of Dzyaloshinskii-Moriya and long-range dipolar interactions as two physical mechanisms determining skyrmion size and stability, a consideration of importance for the optimization of skyrmion characteristics for spintronic applications.

Magnetic skyrmions are a prime example of topologically non-trivial spin textures observed in a variety of magnetic materials. Their nucleation and annihilation in an otherwise uniformly magnetized ferromagnet is enabled by the discrete nature of matter [1–4]. Magnetic skyrmions emerge when the exchange and anisotropy energies promoting parallel alignment of spins in a ferromagnet enter in competition with energies favoring non-collinear alignment of spins such as the Dzyaloshinskii-Moriya interaction (DMI) [5, 6], the long-range dipolar interaction [7, 8] or higher-order exchange interactions [6, 9, 10]. In particular, DMI is at the heart of a large number of magnetic skyrmion observations in recent years. This antisymmetric exchange interaction is related to the lack of structural inversion symmetry and is present in a variety of bulk chiral magnets [11–15]. Interfacial DMI induced by the symmetry breaking in ferromagnetic heterostructures with asymmetric interfaces [16–18] also leads to the formation of skyrmions in thin ferromagnetic layers [1, 19, 20] and multilayers [21].

Another classical energy term well known to favor non-collinear spin alignment in ferromagnets is the dipolar energy, also called stray field or demagnetizing energy [22]. A manifestation of the long-range nature of this energy in thin films with perpendicular magnetic anisotropy is the appearance of micron-sized magnetic bubble domains [8, 23–25]. The equilibrium shape and size of these domains is determined by the balance between the long-range dipolar interaction and the energy cost of the bubble related to the domain wall energy and the Zeeman energy.

*Université de Toulouse, Laboratoire de Physique et Chimie des Nano-Objets, UMR 5215 INSA, CNRS, UPS, 135 Avenue de Rangueil, F-31077 Toulouse Cedex 4, France

†Department of Mathematical Sciences, New Jersey Institute of Technology, Newark, New Jersey 07102, USA. Please use bernandm@insa-toulouse.fr for correspondence.

The original theoretical understanding of skyrmions in ultrathin ferromagnetic layers with interfacial DMI relied on a model that accounts for the dipolar interaction through an effective anisotropy term, neglecting long-range effects [5, 26]. At the same time, in single ferromagnetic layers with interfacial DMI, large chiral skyrmions, also called skyrmionic bubbles have been observed [27–31], suggesting a non-trivial interplay between DMI and long-range dipolar effects. The competition between these two energies also leads to the formation of skyrmions exhibiting spin rotations with intermediate angles between Néel and Bloch [32–34], a phenomenon also present in domain walls [35]. In addition, there is a growing body of theoretical evidence that points to a need to take into account the long-range dipolar energy in the models describing magnetic skyrmions [32, 36–38]. In particular, Büttner et al. [32] used a 360°-wall ansatz [39] to numerically calculate the skyrmion equilibrium radius and energy as functions of the material parameters for intermediate thicknesses, focusing on room temperature stable skyrmions and predicting the existence of room temperature skyrmions stabilized solely by the stray field.

The above considerations put into question the validity of the commonly used assumption that the contribution of the long-range dipolar interaction is negligible. Another open question is whether there exists a size difference between the skyrmions stabilized by the DMI and those stabilized by the stray field [32, 36–38]. In the present work we address these questions rigorously for the first time, using an ansatz-free mathematical analysis of a micromagnetic model that is valid for sufficiently small film thicknesses. We provide explicit analytical expressions for the skyrmion radius, rotation angle and energy valid in the low DMI and thickness regime and taking into account the long-range dipolar energy contribution. We obtain a prediction for the critical DMI value at which the skyrmion character changes from pure Néel to a mixed Néel-Bloch type. These findings are corroborated by micromagnetic simulations. Our rigorous treatment of the stray field contribution sheds light on the necessity to tune both the magnetic layer thickness and the DMI constant to optimise the skyrmion size and stability for applications.

Model

We consider a ferromagnetic thin film with perpendicular magnetic anisotropy (PMA) and infinite extent in the plane. The film is assumed to be sufficiently thin in order for the magnetization vector \mathbf{m} to be constant in the direction normal to the film plane. Under these conditions, the micromagnetic energy [22] reduces to [40–42]:

$$E(\mathbf{m}) = \int_{\mathbb{R}^2} \left(|\nabla \mathbf{m}|^2 + (Q - 1) |\mathbf{m}_{\perp}|^2 + \kappa (m_{\parallel} \nabla \cdot \mathbf{m}_{\perp} - \mathbf{m}_{\perp} \cdot \nabla m_{\parallel}) \right) d^2 r - \frac{\delta}{8\pi} \int_{\mathbb{R}^2} \int_{\mathbb{R}^2} \frac{(m_{\parallel}(\mathbf{r}) - m_{\parallel}(\mathbf{r}'))^2}{|\mathbf{r} - \mathbf{r}'|^3} d^2 r d^2 r' + \frac{\delta}{4\pi} \int_{\mathbb{R}^2} \int_{\mathbb{R}^2} \frac{\nabla \cdot \mathbf{m}_{\perp}(\mathbf{r}) \nabla \cdot \mathbf{m}_{\perp}(\mathbf{r}')}{|\mathbf{r} - \mathbf{r}'|} d^2 r d^2 r'. \quad (1)$$

Here E is measured in the units of Ad , where A is the exchange stiffness and d is the film thickness, lengths are measured in the units of the exchange length $\ell_{ex} = \sqrt{2A/(\mu_0 M_s^2)}$, M_s is the saturation magnetization and $\delta = d/\ell_{ex} \lesssim 1$ is the dimensionless film thickness (for further model details, see Supplementary Information). Furthermore, in Eq. (1) we set $\mathbf{m} = (\mathbf{m}_{\perp}, m_{\parallel})$, where $\mathbf{m}_{\perp} \in \mathbb{R}^2$ and $m_{\parallel} \in \mathbb{R}$ are the respective in-plane and out-of-plane components of \mathbf{m} , and introduced the dimensionless quality factor $Q = K_u/K_d$, where K_u is the magnetocrystalline anisotropy constant, $K_d = \frac{1}{2}\mu_0 M_s^2$, and the dimensionless DMI strength $\kappa = D/\sqrt{AK_d}$. The first three energy terms are local and represent, respectively, the exchange energy, the effective anisotropy energy, which corresponds to the magnetocrystalline energy renormalized to take into account the local stray field contribution, and the DMI energy. The last two terms correspond to the long-range part of the

dipolar energy, which splits into two contributions. The first contribution is due to the out-of-plane component of \mathbf{m} and accounts for surface charges at the top and bottom interfaces of the film. The second energy term corresponds to volume charges and is due to the in-plane divergence of the magnetization.

What is a magnetic skyrmion?

Magnetic skyrmions were originally predicted to exist using a fully local micromagnetic model that is obtained from Eq. (1) by setting $\delta = 0$ [5, 26]. Within this model [43, 44], the ground state for PMA materials ($Q > 1$) and sufficiently small values of $|\kappa|$ is the monodomain state $\mathbf{m} = \pm \hat{\mathbf{z}}$, where $\hat{\mathbf{z}}$ is the unit normal vector to the film plane (the xy -plane) [26, 40]. Therefore, one should identify magnetic skyrmions with metastable magnetization configurations that locally minimize the energy in Eq. (1). In addition, skyrmions possess a non-zero topological charge $q \in \mathbb{Z}$ defined as [45–47]

$$q(\mathbf{m}) = \frac{1}{4\pi} \int_{\mathbb{R}^2} \mathbf{m} \cdot \left(\frac{\partial \mathbf{m}}{\partial x} \times \frac{\partial \mathbf{m}}{\partial y} \right) dx dy \quad \text{for} \quad \lim_{|\mathbf{r}| \rightarrow \infty} \mathbf{m}(\mathbf{r}) = -\hat{\mathbf{z}}, \quad (2)$$

where the last condition fixes the sign convention so that $q = +1$ for either the Néel or Bloch skyrmion profiles. In a fully local micromagnetic model with bulk DMI and no anisotropy term, Melcher [48] studied the existence of minimizers among nontrivial topological sectors in the presence of a sufficiently strong Zeeman term. He found that in this class the energy is globally minimized by a configuration with $q = +1$ (in our convention) and identified this energy minimizing magnetization configuration with a magnetic skyrmion.

In contrast, in the absence of an applied magnetic field and in the presence of long-range dipolar interaction the monodomain state is never the ground state in an extended ferromagnetic film [41, 49]. This can be seen by noting that the energy in Eq. (1) with $Q > 1$ and $\delta > 0$ goes to negative infinity for configurations consisting of a growing bubble domain in which the $\mathbf{m} = +\hat{\mathbf{z}}$ core is separated from the $\mathbf{m} = -\hat{\mathbf{z}}$ background by a Bloch or Néel wall, depending on the magnitude of $|\kappa|$, and which carry the topological charge $q = +1$ [37, 41]. Thus, it is not possible to carry out the analysis of [48] to establish existence of skyrmion profiles via direct energy minimization without introducing further restrictions on the admissible configurations distinguishing compact magnetic skyrmions from skyrmionic bubbles. In the present work, we assign a mathematical meaning to this notion of compact magnetic skyrmion by defining a class of admissible configurations in which the topological charge is fixed to $q = +1$ and the exchange energy cannot exceed twice the topological lower bound, i.e., twice the exchange energy of the Belavin-Polyakov profile [32, 37, 50]. Within this class we establish the existence of compact skyrmions as minimizers of the energy in Eq. (1) for

$$(2|\kappa| + \delta)^2 < 2(Q - 1), \quad (3)$$

which is only a sufficient condition for existence of skyrmion solutions (refer to Methods and Supplementary Information for details).

Skyrmion solution in the low $|\kappa|$ and δ regime

We now proceed with a more detailed description of the obtained solutions. It is known that in a model with exchange energy alone the minimizer is given explicitly by all rigid in-plane rotations, dilations and translations of the Belavin-Polyakov profile [50]. It can be expected that in the

limit where additional energy terms appear as perturbations of the dominating exchange energy, skyrmions retain the Belavin-Polyakov profile [9]. This has been demonstrated recently via a formal asymptotic analysis of radial skyrmion solutions in the local model with bulk DMI in the limit of vanishing DMI constant [51]. In the full model given in Eq. (1), we were able to prove [52] that as $\kappa, \delta \rightarrow 0$ the energy minimizing profile \mathbf{m} converges to a Belavin-Polyakov profile \mathbf{m}_0 given by

$$\mathbf{m}_0(\mathbf{r}) = \left(\frac{2r_0 R_{\theta_0} \mathbf{r}}{|\mathbf{r}|^2 + r_0^2}, \frac{r_0^2 - |\mathbf{r}|^2}{r_0^2 + |\mathbf{r}|^2} \right) \quad \mathbf{r} \in \mathbb{R}^2, \quad (4)$$

where R_{θ_0} is the 2×2 matrix of in-plane rotations by angle

$$\theta_0 = \begin{cases} 0 & \text{if } \kappa \geq \frac{3\pi^2}{32}\delta, \\ -\pi & \text{if } \kappa \leq -\frac{3\pi^2}{32}\delta, \\ \pm \arccos\left(\frac{32\kappa}{3\pi^2\delta}\right) & \text{else,} \end{cases} \quad (5)$$

and the dimensionless skyrmion radius is asymptotically

$$r_0 \simeq \frac{1}{16\pi\sqrt{Q-1}} \times \frac{\bar{\varepsilon}(\kappa, \delta, Q)}{|\log(\beta\bar{\varepsilon}(\kappa, \delta, Q))|}, \quad (6)$$

for $\beta\bar{\varepsilon} \ll 1$ with $\beta \approx 0.0174$ and

$$\bar{\varepsilon}(\kappa, \delta, Q) = \frac{1}{\sqrt{Q-1}} \times \begin{cases} \left(8\pi|\kappa| - \frac{\pi^3}{4}\delta\right) & \text{if } |\kappa| \geq \frac{3\pi^2}{32}\delta, \\ \left(\frac{128\kappa^2}{3\pi\delta} + \frac{\pi^3}{8}\delta\right) & \text{else.} \end{cases} \quad (7)$$

The above expressions may be obtained by considering a suitably truncated magnetization profile in the form of Eq. (4), optimizing in θ_0 and r_0 and expanding the obtained expressions in the leading order of δ and $|\kappa|$ (see Supplementary Information for more details). Our analysis also yields the following asymptotic expression for the skyrmion energy:

$$E_0 \simeq 8\pi - \frac{\bar{\varepsilon}^2(\kappa, \delta, Q)}{32\pi|\log(\beta\bar{\varepsilon}(\kappa, \delta, Q))|}. \quad (8)$$

The associated skyrmion collapse energy barrier $\Delta E_0 = E_0 - 8\pi$ gives an indication of the skyrmion stability as it represents the energy necessary to suppress the skyrmion via compression [3, 32, 37]. The solution described in Eqs. (4)–(8) is asymptotically exact to the leading order for $|\kappa| \ll \sqrt{Q-1}$ and $\delta \ll \sqrt{Q-1}$, but in practice remains at least qualitatively correct also up to $\kappa \sim \sqrt{Q-1}$ and $\delta \sim \sqrt{Q-1}$.

Dependence of the skyrmion characteristics on the parameters

The dependences of the dimensionless skyrmion radius r_0 , the collapse energy ΔE_0 and the rotation angle θ_0 on the model parameters are presented in Fig. 1 (see Supplementary Information for the precise analytical expressions being plotted). The first important characteristic of the solution is the existence of a minimum or threshold $|\kappa|$ value

$$|\kappa|_{\text{sky}}^{\text{thresh}} = \frac{3\pi^2}{32}\delta, \quad (9)$$

above which pure Néel skyrmions ($\theta_0 = 0$) are obtained and below which skyrmions are characterized by a non-zero rotation angle θ_0 . This angle tends to $\pm\pi/2$, corresponding to pure Bloch

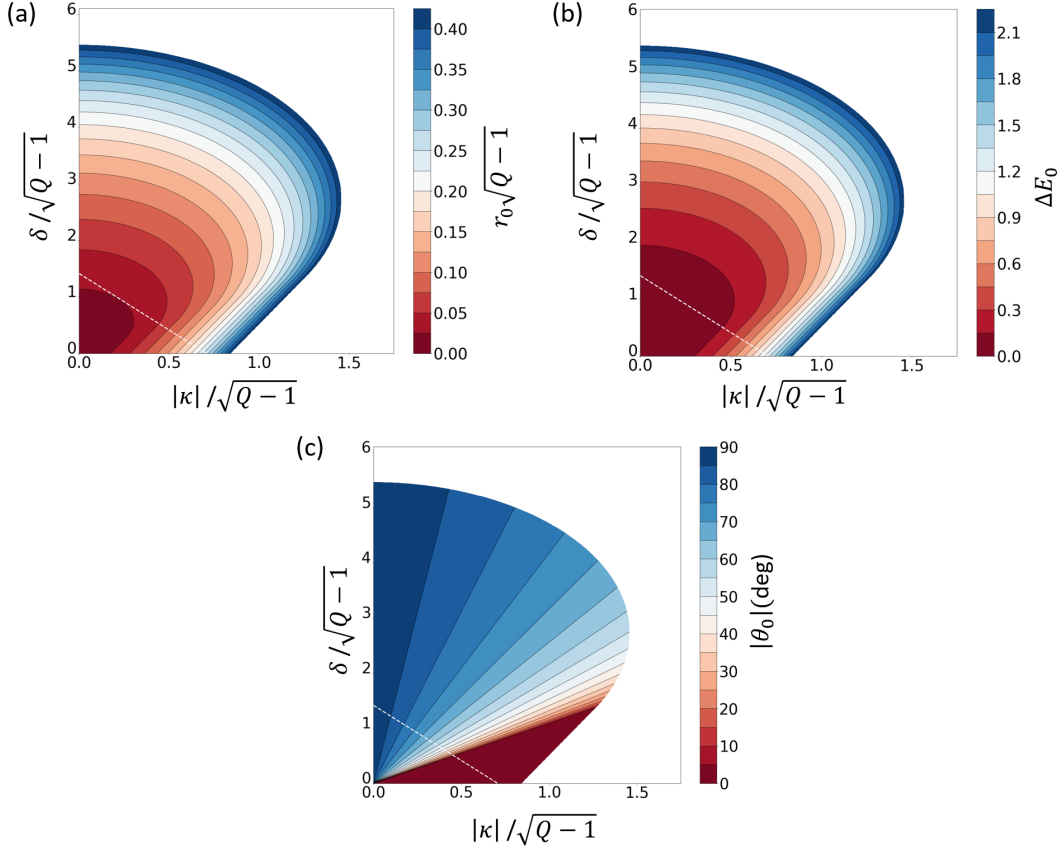


Figure 1: Dependences of the skyrmion characteristics on the parameters obtained using a suitably truncated ansatz from Eq. (4): (a) the dimensionless skyrmion radius r_0 ; (b) the skyrmion collapse energy barrier ΔE_0 ; and (c) the rotation angle $|\theta_0|$ from Eq. (5) (for the precise analytical expressions for r_0 and ΔE_0 being plotted, see Supplementary Information); these expressions are well approximated by the ones in Eqs. (6) and (8) for $|\kappa|, \delta \lesssim \sqrt{Q-1}$. The dark red region in panel (c) indicates purely Néel skyrmions. The rest of the parameter region corresponds to mixed Néel-Bloch skyrmions, with pure Bloch skyrmions for $\kappa = 0$ stabilized solely by dipolar interactions. The dashed white line corresponds to the boundary of the region defined in Eq. (3), in which existence of skyrmion solutions is guaranteed.

skyrmions when $\kappa \rightarrow 0$. It is a direct consequence of the competition between long-range dipolar interaction, which favors a Bloch rotation, and interfacial DMI, which favors a Néel rotation. Note that a similar threshold is observed in the case of straight domain walls [35, 53]:

$$|\kappa|_{\text{wall}}^{\text{thresh}} = \frac{4 \ln 2}{\pi^2} \delta. \quad (10)$$

Thus, a larger DMI is necessary to obtain a pure Néel skyrmion as compared to the case of a 1D Néel wall, as can be seen from the factor of ~ 3 difference between Eqs. (9) and (10). This is an indication that dipolar effects play a stronger role for skyrmions compared to domain walls.

Another characteristic associated with the interplay between DMI and the dipolar interaction that is visible in Figs. 1a and 1b is the non-monotone dependence of the dimensionless skyrmion radius r_0 and collapse energy ΔE_0 on δ for Q and κ fixed. For δ below the critical value where skyrmions are of Néel character, the skyrmion radius decreases with increasing δ , while for large enough δ , in the regime with non-zero θ_0 , the radius increases with δ . This observation is of importance for applications, as the thickness of the film is the parameter which is the most easy to tune experimentally for a thin film in order to optimize the skyrmion size and stability. A practical example in the case of a ferrimagnetic film will be given in the section preceding the summary.

The third important result illustrated in Fig. 1 is the existence of skyrmions stabilized solely by the long-range dipolar interaction for $\kappa = 0$. Such dipolar skyrmions possess a pure Bloch character ($\theta_0 = \pm\pi/2$), with volume charges not contributing to the energy. We observe in Fig. 1a that, starting from $\kappa = 0$ and following a skyrmion solution of fixed radius while decreasing δ , one goes continuously from a Bloch skyrmion at $\kappa = 0$ to a Néel skyrmion at $\delta = 0$. Consequently, skyrmions stabilized by DMI and stray field cannot be distinguished by their radius.

Position of the skyrmion solutions on a skyrmion phase diagram

To complete our description, we locate the skyrmion solutions on a phase diagram (see Fig. 2a). For that purpose, we fix the film thickness and DMI constant to $d = 1$ nm and $D = 0.5$ mJ/m², respectively, and vary the saturation magnetization M_s and magnetocrystalline anisotropy constant K_u over a wide range. The solid black line represents the threshold at which the magnetization reorientation transition between in-plane and out-of-plane occurs at $Q = 1$, i.e., for $K_u = K_d$. In the dark blue region above this line, the magnetization prefers to lie in the film plane, and no compact skyrmion solutions exist in an infinite film. Below this line, the easy axis is perpendicular to the film plane. In the zone represented in light blue, the domain wall energy density defined as $\sigma_{\text{wall}} = 4\sqrt{A(K_u - K_d)} - \pi D$ is negative. Here, the expected ground state of the ferromagnetic thin film is the helicoidal state [54], and compact skyrmions do not exist in the absence of an applied magnetic field [1]. Below the dashed blue line corresponding to $K_u^{\text{crit}} = \frac{\pi^2 D^2}{16A} + K_d$, the domain wall energy becomes positive again, and compact skyrmions may exist as metastable states. In the light red region, the existence of axisymmetric compact skyrmions is, however, not guaranteed, as elongated objects (stripes) may be more energetically favorable [55]. The dark red zone represents the domain of existence of our skyrmion solutions. It is delimited by a dashed black line, which represents the boundary of the region defined by Eq. (3) below which we have existence of a compact skyrmion. When the anisotropy is further increased (or M_s is decreased), the limit of validity of our 2D thin film model is reached as the skyrmion radius becomes of the order of the film thickness. The white dashed line represents the line at which $r_{\text{sky}} = d$ as a guide to the eye.

In Fig. 2b, the radius of the skyrmion solutions is plotted for different D values at a fixed thickness of $d = 1$ nm. When D is decreased from 1 mJ/m² to 0.5 mJ/m² the skyrmion solutions

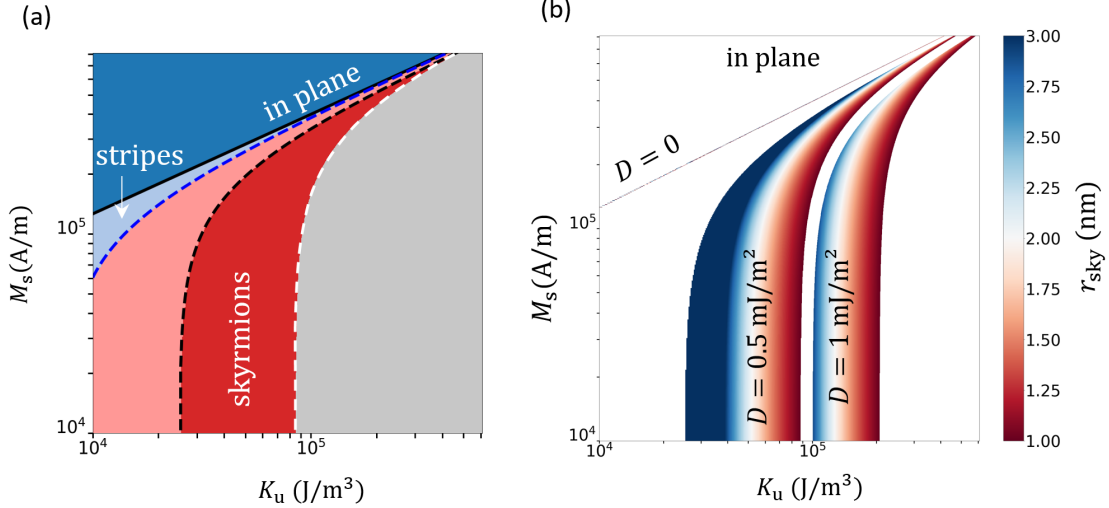


Figure 2: Skymion phase diagrams calculated at fixed thickness $d = 1$ nm and exchange stiffness $A = 20$ pJ/m as functions of a wide range of magnetization M_s and uniaxial anisotropy K_u values. (a) Phase diagram for $D = 0.5$ mJ/m², where our solutions appear in the dark red zone. (b) Skymion radius r_{sky} calculated for three D values. In (a), the solid black line corresponds to the spin reorientation transition at $K_u = K_d$, the dashed blue line indicates the critical K_u value $K_u^{crit} = \frac{\pi^2 D^2}{16A} + K_d$ below which the 1D wall energy becomes negative, the dashed black line represents the existence limit from Eq. (3), and the grey zone corresponds to solutions with $r_{sky} < d$.

shift to lower K_u values, as K_u^{crit} is decreased. We observe that low M_s values increase the K_u range in which compact skymions solutions are observed, as also reported by Büttner et al. [32]. Consequently, in materials with high M_s stripe patterns are more likely to be observed than isolated skymions at zero magnetic field, and a sufficiently strong magnetic field needs to be applied to allow the existence of isolated skymions, as observed experimentally [1]. For $D = 0$ the solutions are restricted to a very narrow M_s and K_u range close to the out-of-plane to in-plane transition line. Indeed, at small thickness (e.g., $d = 1$ nm used in Fig. 2), the long-range dipolar energy becomes comparable to the anisotropy energy only in the case of a low effective anisotropy $K_{eff} = K_u - K_d \ll K_d$. Skymions for $D = 0$ can be expected to exist for a wider range of M_s and K_u values when the layer thickness is increased, since the strength of the long-range dipolar interaction increases with the thickness in the thin film regime.

Application to specific examples for low and intermediate D values

In this section, we apply our compact skymion results to the case of *ferrimagnetic* materials, i.e., materials with low M_s and K_u values (e.g., GdCo). These conditions favor the observation of skymions in the absence of an applied magnetic field, as was recently reported [32, 56] and as discussed in the previous section.

In Fig. 3, we present the case of low D values and $Q = 1.01$, for which the transition from pure Néel to pure Bloch skymion appears, as seen in Fig. 3c. For comparison, we carried out micromagnetic simulations at fixed D for two thicknesses represented by white dots in Fig. 3a,c (see Methods for details on the simulation). At $d = 1$ nm, both the simulations and the analysis predict a Néel skymion. At $d = 5$ nm, we obtain a skymion with a rotation angle $\theta_0 \simeq 60^\circ$

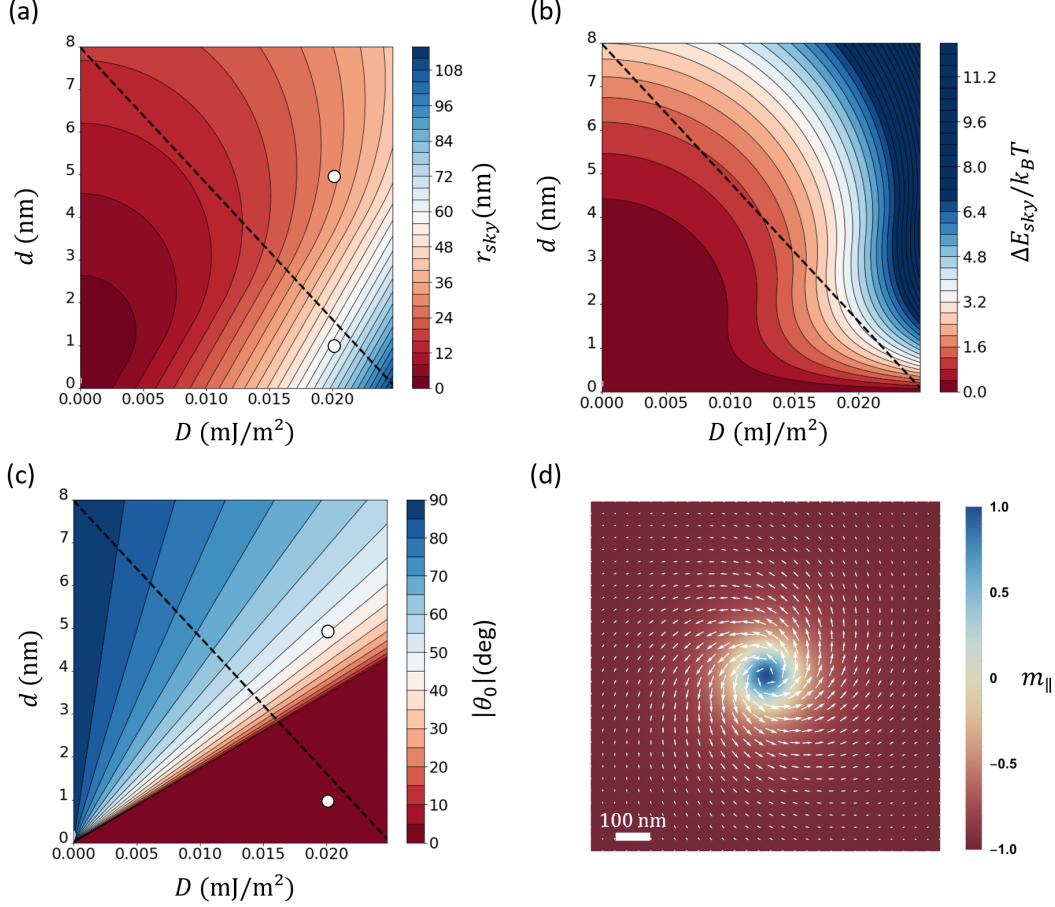


Figure 3: Dependences of the skyrmion characteristics in the low DMI regime. The other parameters are fixed to $A = 20$ pJ/m, $M_s = 10^5$ A/m, and $K_u = 6346$ J/m³ corresponding to $Q = 1.01$. (a) The skyrmion radius r_{sky} . (b) The normalized skyrmion collapse energy barrier $\Delta E_{\text{sky}}/k_B T$, where k_B is the Boltzmann constant and $T = 293$ K. (c) The rotation angle $|\theta_0|$. In (a)–(c), the black dashed line indicates the limit of existence region defined in Eq. (3). The white dots in (a) and (c) mark the parameters for which micromagnetic simulations discussed in the text were carried out. (d) A skyrmion solution obtained from a micromagnetic simulation with the same parameters as in (a), $d = 5$ nm and $D = 0.02$ mJ/m², corresponding to the upper white dot in (a) and (c) (see Methods for details). The image in (d) is constructed by superimposing the in-plane magnetization \mathbf{m}_\perp represented with arrows and the out-of-plane magnetization m_\parallel represented by a colormap.

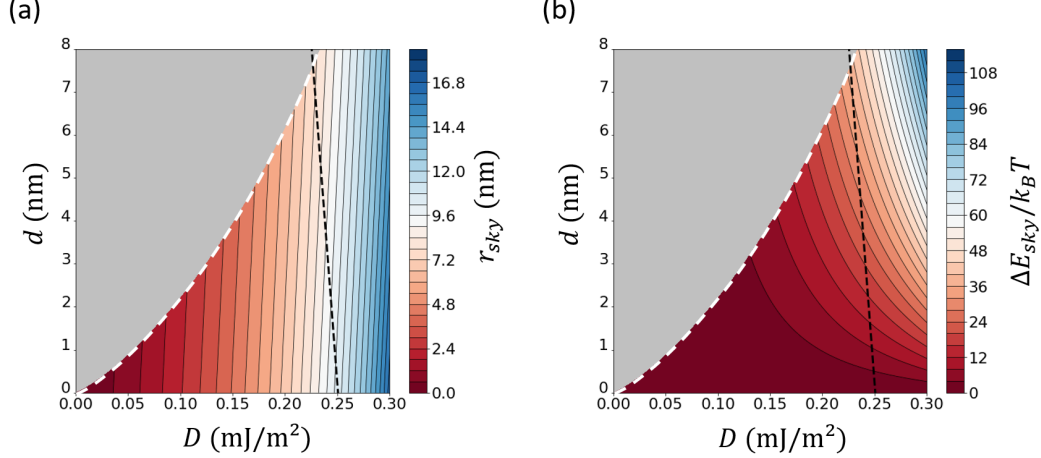


Figure 4: Dependences of the skyrmion characteristics in the intermediate DMI regime. The other parameters are fixed to $A = 20$ pJ/m, $M_s = 10^5$ A/m, and $K_u = 1.26 \times 10^4$ J/m³ corresponding to $Q = 2$. The black dashed line indicates the limit of existence defined in Eq. (3). (a) The skyrmion radius r_{sky} . (b) The normalized skyrmion collapse energy barrier $\Delta E_{\text{sky}}/k_B T$, where k_B is the Boltzmann constant and $T = 293$ K. All skyrmions are of Néel type.

from the simulations presented in Fig. 3d, vs. $\theta_0 \simeq 46^\circ$ from our formula. This confirms the transition from purely Néel to intermediate Néel-Bloch rotation angle predicted by our analysis upon thickness increase. As Néel walls are expected up to thicknesses of ~ 10 nm for 1D walls (see Eq. (10)), this observation of a skyrmion with an intermediate rotation angle at $d = 5$ nm validates the increased importance of dipolar interaction in the case of compact skyrmions predicted by our theory compared to 1D walls.

Fig. 3b shows the skyrmion collapse energy barrier $\Delta E_{\text{sky}} = \Delta E_0 A d$ normalized by the room temperature thermal energy $k_B T$, where k_B is the Boltzmann constant and $T = 293$ K. We point out that the lifetime of Néel skyrmions is significantly increased upon increasing the film thickness due to the dimensional scale factor of Ad . Conversely, the Ad factor is also responsible for the short skyrmion lifetime (< 1 s) observed in ferromagnetic monolayers with $d \sim 0.3$ nm [1]. This consideration justifies the choice of systems with bulk out-of-plane anisotropy (like the ferrimagnetic alloy GdCo) or multilayers (e.g., (Pt/Co/Ir)_n) to optimise skyrmion lifetime, since they allow to increase the film thickness (or effective thickness) without losing the out-of-plane anisotropy, as would be the case for single ferromagnetic layers with surface-induced anisotropy alone.

In Fig. 4, we present the results for an intermediate DMI range where the D values are an order of magnitude larger than those in Fig. 3, now with $Q = 2$. All the solutions in Fig. 4 are iconic Néel skyrmions with $\lesssim 10$ nm radius that grows with an increase of the DMI strength. The skyrmion collapse barrier can be heightened by either increasing the film thickness or the DMI strength (Fig. 4b), and the collapse energy barrier reaches $32 k_B T$ ($\sim 10^6$ s lifetime, considering the Néel-Brown model) for skyrmion radius < 10 nm. Such a small size and high stability are promising in terms of applications for information technology [57]. At fixed thickness d , the skyrmion radius decreases with the DMI, and the limit of validity of our thin film model is reached as the skyrmion radius becomes of the same order as the film thickness. In this regime, 3D models and full 3D micromagnetic simulations will be needed to take into account the long-range dipolar effects.

Summary

We have used mathematical analysis to develop a skyrmion theory that takes into account the full dipolar energy in the thin film regime. While long-range interactions are often assumed to have a negligible impact on skyrmions in this regime, we rigorously demonstrate that the DMI threshold at which a compact skyrmion loses its Néel character is a factor of ~ 3 lower than that for a 1D wall. Consequently, a reorientation of the skyrmion rotation angle from Néel to intermediate Néel-Bloch angles is predicted as the layer thickness is increased in the low DMI regime, which is confirmed by numerical simulations. This conclusion is particularly relevant for applications, since an increase in the film thickness (or effective thickness) is the main way to increase the skyrmion lifetime while preserving its nanometer dimensions. Importantly, a thickness increase is potentially associated with a strong decrease in the DMI strength due to the interfacial origin of the latter in the considered systems. This makes our analytical formulas a powerful tool to predict the parametric dependence of skyrmion size and lifetime, and serve as a starting point for more time-consuming numerical simulations and material engineering.

Methods

Mathematical analysis

In search for a suitable condition that would pinpoint compact skyrmions and distinguish them from both bubbles or more exotic states such as skyrmion bags [47, 58], we turn to the notion of the topological lower bound, which states that the exchange energy of a topologically nontrivial configuration is bounded below by a constant depending only on the topological charge [48, 50]:

$$\int_{\mathbb{R}^2} |\nabla \mathbf{m}|^2 d^2r \geq 8\pi |q(\mathbf{m})| \quad (11)$$

for all $\mathbf{m} \in \dot{H}^1(\mathbb{R}^2; \mathbb{S}^2)$, i.e., in the space of vector-valued functions in the plane with unit length constraint and for which the left-hand side in Eq. (11) is well-defined and finite. In particular, for all configurations with $q \neq \{0, \pm 1\}$ the exchange energy is bounded below by 16π . Therefore, we can exclude all these configurations by restricting the admissible configurations to those that satisfy

$$\int_{\mathbb{R}^2} |\nabla \mathbf{m}|^2 d^2r < 16\pi. \quad (12)$$

Note that this also rules out large bubble domains with topological charge $q = +1$ mentioned earlier, as the exchange energy in those configurations would be large proportionally to the bubble radius [22, 37]. Thus, any minimizer of the energy in Eq. (1) with topological charge $q \neq 0$ and satisfying Eq. (12) must necessarily be either a compact skyrmion ($q = +1$) or an antiskyrmion ($q = -1$). In fact, the condition in Eq. (12) together with the choice of $q = +1$ can be taken as the definition of a compact magnetic skyrmion. For that purpose, we introduce the following class of admissible configurations over which the minimization is carried out:

$$\mathcal{A}_{+1} = \left\{ \mathbf{m} \in \dot{H}^1(\mathbb{R}^2; \mathbb{S}^2) : \mathbf{m} + \hat{\mathbf{z}} \in L^2(\mathbb{R}^2; \mathbb{R}^3), q(\mathbf{m}) = +1, \int_{\mathbb{R}^2} |\nabla \mathbf{m}|^2 d^2r < 16\pi \right\}. \quad (13)$$

Note that in addition to Eq. (12) and the conditions already discussed, we also demand square integrability of $\mathbf{m} + \hat{\mathbf{z}}$, which forces $\mathbf{m}(\mathbf{r})$ to approach $-\hat{\mathbf{z}}$ at least in some average sense as $|\mathbf{r}| \rightarrow \infty$. This is needed, because E does not distinguish between configurations differing only by the sign of \mathbf{m} . We then have the following result.

Theorem 1. *Let $Q > 1$, $\delta > 0$ and $\kappa \in \mathbb{R}$ be such that Eq. (3) holds. Then there exists $\mathbf{m}^* \in \mathcal{A}_{+1}$ such that $E(\mathbf{m}^*) = \min_{\mathbf{m} \in \mathcal{A}_{+1}} E(\mathbf{m})$.*

A sketch of the proof of this theorem is presented in the Supplementary Information. Let us point out that the obtained minimizer indeed has topological charge $q = +1$ and has the shape of a localized perturbation of the ground state $\mathbf{m} = -\hat{\mathbf{z}}$. In particular, it is a stable stationary solution of the Landau-Lifshitz-Gilbert equation that converges to $-\hat{\mathbf{z}}$ at infinity. We note that in the proof the condition in Eq. (12) ensures that one cannot lower the energy by splitting one skyrmion into two compact, well separated objects with topological charges adding up to $+1$ (say, $+2$ and -1). The condition appearing in Eq. (3) ensures that the exchange energy dominates the DMI and the dipolar energies and guarantees that the condition in Eq. (12) remains valid when passing to the limit in a minimizing sequence.

Micromagnetic simulations

We carried out micromagnetic simulations using MuMax3 [59]. The system is a $4096 \times 4096 \text{ nm}^2$ square box with a mesh size of $4 \times 4 \times 5 \text{ nm}^3$ subject to periodic boundary conditions. The parameters are the same as in Fig. 3, namely, $A = 20 \text{ pJ/m}$, $M_s = 10^5 \text{ A/m}$ and $K_u = 6346 \text{ J/m}^3$. For $d = 5 \text{ nm}$ and $D = 0.02 \text{ mJ/m}^2$ we obtain a skyrmion with $\theta_0 \simeq 60^\circ$ and $r_{\text{sky}} \simeq 80 \text{ nm}$. For $d = 1 \text{ nm}$ and $D = 0.02 \text{ mJ/m}^2$ we obtain a skyrmion with $\theta_0 \simeq 0^\circ$ and $r_{\text{sky}} \simeq 120 \text{ nm}$.

Acknowledgements

A. B.-M. wishes to acknowledge support from DARPA TEE program through grant MIPR#HR0011831554. The work of C. B. M. and T. M. S. was supported, in part, by NSF via grants DMS-1614948 and DMS-1908709. C. B. M. would also like to thank the LABEX NEXT “Nano, Mesures EXtrêmes et Théorie” ANR-10-LABX-0037-NEXT for financial support, and LPCNO, INSA, Toulouse, France, where part of this work was done, for its hospitality.

References

- [1] N. Romming, C. Hanneken, M. Menzel, J. E. Bickel, B. Wolter, K. von Bergmann, A. Kubetzka, and R. Wiesendanger. Writing and deleting single magnetic skyrmions. *Science*, 341:636–639, 2013.
- [2] Alberto D. Verga. Skyrmion to ferromagnetic state transition: A description of the topological change as a finite-time singularity in the skyrmion dynamics. *Phys. Rev. B*, 90:174428, 2014.
- [3] D. Cortés-Ortuño, W. Wang, M. Beg, R. A. Pepper, M.-A. Bisotti, R. Carey, M. Vousden, T. Kluyver, O. Hovorka, and H. Fangohr. Thermal stability and topological protection of skyrmions in nanotracks. *Sci. Rep.*, 7:4060, 2017.
- [4] J. Hagemeister, N. Romming, K. von Bergmann, E. Y. Vedmedenko, and R. Wiesendanger. Stability of single skyrmionic bits. *Nature Commun.*, 6:8455, 2015.
- [5] A. N. Bogdanov and D. A. Yablonskii. Thermodynamically stable “vortices” in magnetically ordered crystals. The mixed state of magnets. *Sov. Phys. – JETP*, 68:101–103, 1989.
- [6] B. Ivanov, V. Stephanovich, and A. Zhmudskii. Magnetic vortices: The microscopic analogs of magnetic bubbles. *J. Magn. Magn. Mater.*, 88:116–120, 1990.

- [7] X. Z. Yu, K. Shibata, W. Koshibae, Y. Tokunaga, Y. Kaneko, T. Nagai, K. Kimoto, Y. Taguchi, N. Nagaosa, and Y. Tokura. Thermally activated helicity reversals of skyrmions. *Phys. Rev. B*, 93:134417, 2016.
- [8] S. A. Montoya, S. Couture, J. J. Chess, J. C. T. Lee, N. Kent, D. Henze, S. K. Sinha, M.-Y. Im, S. D. Kevan, P. Fischer, B. J. McMorran, V. Lomakin, S. Roy, and E. E. Fullerton. Tailoring magnetic energies to form dipole skyrmions and skyrmion lattices. *Phys. Rev. B*, 95:024415, 2017.
- [9] A. Abanov and V. L. Pokrovsky. Skyrmion in a real magnetic film. *Phys. Rev. B*, 58:R8889, 1998.
- [10] T. Okubo, S. Chung, and H. Kawamura. Multiple-q states and the skyrmion lattice of the triangular-lattice Heisenberg antiferromagnet under magnetic fields. *Phys. Rev. Lett.*, 108:017206, 2012.
- [11] S. Mühlbauer, B. Binz, F. Jonietz, C. Pfleiderer, A. Rosch, A. Neubauer, R. Georgii, and P. Böni. Skyrmion lattice in a chiral magnet. *Science*, 323:915–919, 2009.
- [12] X. Z. Yu, Y. Onose, N. Kanazawa, J. H. Park, J. H. Han, Y. Matsui, N. Nagaosa, and Y. Tokura. Real-space observation of a two-dimensional skyrmion crystal. *Nature*, 465:901–904, 2010.
- [13] Y. Tokunaga, X. Z. Yu, J. S. White, H. M. Ronnow, D. Morikawa, Y. Taguchi, and Y. Tokura. A new class of chiral materials hosting magnetic skyrmions beyond room temperature. *Nature Commun.*, 6:7638, 2015.
- [14] I. Kézsmárki, S. Bordács, P. Milde, E. Neuber, L. M. Eng, J. S. White, H. M. Rønnow, C. D. Dewhurst, M. Mochizuki, K. Yanai, H. Nakamura, D. Ehlers, V. Tsurkan, and A. Loidl. Néel-type skyrmion lattice with confined orientation in the polar magnetic semiconductor GaV_4S_8 . *Nature Mat.*, 14:1116–1122, 2015.
- [15] S. Seki, X. Z. Yu, S. Ishiwata, and Y. Tokura. Observation of skyrmions in a multiferroic material. *Science*, 336:198–201, 2012.
- [16] M. Bode, M. Heide, K. von Bergmann, P. Ferriani, S. Heinze, G. Bihlmayer, A. Kubetzka, O. Pietzsch, S. Blugel, and R. Wiesendanger. Chiral magnetic order at surfaces driven by inversion asymmetry. *Nature*, 447:190–193, 2007.
- [17] M. Heide, G. Bihlmayer, and S. Blügel. Describing Dzyaloshinskii-Moriya spirals from first-principles. *Physica B*, 404:2678–2683, 2009.
- [18] H. Yang, A. Thiaville, S. Rohart, A. Fert, and M. Chshiev. Anatomy of Dzyaloshinskii-Moriya interaction at Co/Pt interfaces. *Phys. Rev. Lett.*, 115:267210, 2015.
- [19] S. Heinze, K. von Bergmann, M. Menzel, J. Brede, A. Kubetzka, R. Wiesendanger, G. Bihlmayer, and S. Blugel. Spontaneous atomic-scale magnetic skyrmion lattice in two dimensions. *Nature Phys.*, 7:713–718, 2011.
- [20] M. Hervé, B. Dupé, R. Lopes, M. Böttcher, M. D. Martins, T. Balashov, L. Gerhard, J. Sinova, and W. Wulfhekel. Stabilizing spin spirals and isolated skyrmions at low magnetic field exploiting vanishing magnetic anisotropy. *Nature Commun.*, 9:1015, 2018.

- [21] C. Moreau-Luchaire, C. Moutafis, N. Reyren, J. Sampaio, N. Van Horne, C. A. F. Vaz, K. Bouzehouane, K. Garcia, C. Deranlot, P. Warnicke, P. Wohlhüter, J. M. George, J. Raabe, V. Cros, and A. Fert. Skyrmions at room temperature: From magnetic thin films to magnetic multilayers. *Nature Nanotechnol.*, 11:444–448, 2016.
- [22] A. Hubert and R. Schäfer. *Magnetic Domains*. Springer, Berlin, 1998.
- [23] C. Kooy and U.ENZ. Experimental and theoretical study of the domain configuration in thin layers of BaFe₁₂O₁₉. *Philips Res. Repts.*, 15:7–29, 1960.
- [24] A.H. Bobeck. Properties and device applications of magnetic domains in orthoferrites. *Bell System. Tech. J.*, 46:1901–1925, 1967.
- [25] P. Chaudhari, J. J. Cuomo, and R. J. Gambino. Amorphous metallic films for magnetooptic applications. *Appl. Phys. Lett.*, 22:337–339, 1973.
- [26] A. Bogdanov and A. Hubert. Thermodynamically stable magnetic vortex states in magnetic crystals. *J. Magn. Magn. Mater.*, 138:255–269, 1994.
- [27] W. Jiang, P. Upadhyaya, W. Zhang, G. Yu, M. B. Jungfleisch, F. Y. Fradin, J. E. Pearson, Y. Tserkovnyak, K. L. Wang, O. Heinonen, S. G. E. te Velthuis, and A. Hoffmann. Blowing magnetic skyrmion bubbles. *Science*, 349:283–286, 2015.
- [28] F. Büttner, C. Moutafis, M. Schneider, B. Kruger, C. M. Gunther, J. Geilhufe, C. v. Korff Schmising, J. Mohanty, B. Pfau, S. Schaffert, A. Bisig, M. Foerster, T. Schulz, C. A. F. Vaz, J. H. Franken, H. J. M. Swagten, M. Kläui, and S. Eisebitt. Dynamics and inertia of skyrmionic spin structures. *Nature Phys.*, 11:225–228, 2015.
- [29] S. Woo, K. Litzius, B. Kruger, M.-Y. Im, L. Caretta, K. Richter, M. Mann, A. Krone, R. M. Reeve, M. Weigand, P. Agrawal, I. Lemesch, M.-A. Mawass, P. Fischer, M. Kläui, and G. S. D. Beach. Observation of room-temperature magnetic skyrmions and their current-driven dynamics in ultrathin metallic ferromagnets. *Nature Mat.*, 15:501–506, 2016.
- [30] G. Yu, P. Upadhyaya, X. Li, W. Li, W. K. Kim, Y. Fan, K. L. Wong, Y. Tserkovnyak, P. K. Amiri, and K. L. Wang. Room-temperature creation and spin-orbit torque manipulation of skyrmions in thin films with engineered asymmetry. *Nano Lett.*, 16:1981–1988, 2016.
- [31] M. Schott, A. Bernand-Mantel, L. Ranno, S. Pizzini, J. Vogel, H. Béa, C. Baraduc, S. Auffret, G. Gaudin, and D. Givord. The skyrmion switch: Turning magnetic skyrmion bubbles on and off with an electric field. *Nano Lett.*, 17:3006–3012, 2017.
- [32] F. Büttner, I. Lemesch, and G. S. D. Beach. Theory of isolated magnetic skyrmions: From fundamentals to room temperature applications. *Sci. Rep.*, 8:4464, 2018.
- [33] W. Legrand, J.-Y. Chauleau, D. Maccariello, N. Reyren, S. Collin, K. Bouzehouane, N. Jaouen, V. Cros, and A. Fert. Hybrid chiral domain walls and skyrmions in magnetic multilayers. *Sci. Adv.*, 4:eaat0415, 2018.
- [34] Y. Dovzhenko, F. Casola, S. Schlotter, T. X. Zhou, F. Büttner, R. L. Walsworth, G. S. D. Beach, and A. Yacoby. Magnetostatic twists in room-temperature skyrmions explored by nitrogen-vacancy center spin texture reconstruction. *Nature Commun.*, 9:2712, 2018.

- [35] A. Thiaville, S. Rohart, E. Jué, V. Cros, and A. Fert. Dynamics of Dzyaloshinskii domain walls in ultrathin magnetic films. *Europhys. Lett.*, 100:57002, 2012.
- [36] N. S. Kiselev, A. N. Bogdanov, R. Schäfer, and U. K. Rößler. Chiral skyrmions in thin magnetic films: new objects for magnetic storage technologies? *J. Phys. D: Appl. Phys.*, 44:392001, 2011.
- [37] A. Bernand-Mantel, L. Camosi, A. Wartelle, N. Rougemaille, M. Darques, and L. Ranno. The skyrmion-bubble transition in a ferromagnetic thin film. *SciPost. Phys.*, 4:027, 2018.
- [38] W. Legrand, N. Ronceray, N. Reyren, D. MacCariello, V. Cros, and A. Fert. Modeling the shape of axisymmetric skyrmions in magnetic multilayers. *Phys. Rev. Appl.*, 10:064042, 2018.
- [39] H.-B. Braun. Fluctuations and instabilities of ferromagnetic domain-wall pairs in an external magnetic field. *Phys. Rev. B*, 50:16485–16500, 1994.
- [40] C. B. Muratov and V. V. Slustikov. Domain structure of ultrathin ferromagnetic elements in the presence of Dzyaloshinskii-Moriya interaction. *Proc. R. Soc. Lond. Ser. A*, 473:20160666, 2016.
- [41] H. Knüpfer, C. B. Muratov, and F. Nolte. Magnetic domains in thin ferromagnetic films with strong perpendicular anisotropy. *Arch. Rat. Mech. Anal.*, 232:727–761, 2019.
- [42] C. B. Muratov. A universal thin film model for Ginzburg-Landau energy with dipolar interaction. *Calc. Var. Partial Differential Equations*, 58:52, 2019.
- [43] J. M. Winter. Bloch wall excitation. Application to nuclear resonance in a Bloch wall. *Phys. Rev.*, 124:452–459, 1961.
- [44] G. Gioia and R. D. James. Micromagnetics of very thin films. *Proc. R. Soc. Lond. Ser. A*, 453:213–223, 1997.
- [45] N. Nagaosa and Y. Tokura. Topological properties and dynamics of magnetic skyrmions. *Nature Nanotechnol.*, 8:899–911, 2013.
- [46] H.-B. Braun. Topological effects in nanomagnetism: from superparamagnetism to chiral quantum solitons. *Adv. Phys.*, 61:1–116, 2012.
- [47] F. N. Rybakov and N. S. Kiselev. Chiral magnetic skyrmions with arbitrary topological charge. *Phys. Rev. B*, 99:064437, 2019.
- [48] C. Melcher. Chiral skyrmions in the plane. *Proc. R. Soc. Lond. Ser. A*, 470:0394 pp. 1–17, 2014.
- [49] B. Kaplan and G. A. Gehring. The domain structure in ultrathin magnetic films. *J. Magn. Mater.*, 128:111–116, 1993.
- [50] A. A. Belavin and A. M. Polyakov. Metastable states of two-dimensional isotropic ferromagnets. *JETP Lett.*, 22:245–247, 1975.
- [51] S. Komineas, C. Melcher, and S. Venakides. The profile of chiral skyrmions. arXiv:1904.01408, 2019.

- [52] A. Bernand-Mantel, C. B. Muratov, and T. M. Simon. A quantitative description of skyrmions in ultrathin ferromagnetic films and stability of degree ± 1 harmonic maps from \mathbb{R}^2 to \mathbb{S}^2 . In preparation.
- [53] I. Lemesch, F. Büttner, and G. S. D. Beach. Accurate model of the stripe domain phase of perpendicularly magnetized multilayers. *Phys. Rev. B*, 95:174423, 2017.
- [54] A. Bogdanov and A. Hubert. The stability of vortex-like structures in uniaxial ferromagnets. *J. Magn. Magn. Mater.*, 195:182–192, 1999.
- [55] A. O. Leonov, T. L. Monchesky, N. Romming, A. Kubetzka, A. N. Bogdanov, and R. Wiesendanger. The properties of isolated chiral skyrmions in thin magnetic films. *New J. Phys.*, 18:065003, 2016.
- [56] L. Caretta, L. Mann, F. Büttner, K. Ueda, B. Pfau, C. M. Günther, P. Hession, A. Churikova, C. Klose, M. Schneider, D. Engel, C. Marcus, D. Bono, K. Bagschik, S. Eisebitt, and G. S. D. Beach. Fast current-driven domain walls and small skyrmions in a compensated ferrimagnet. *Nature Nanotechnol.*, 13:1154–1160, 2018.
- [57] R. Tomasello, E. Martinez, R. Zivieri, L. Torres, M. Carpentieri, and G. Finocchio. A strategy for the design of skyrmion racetrack memories. *Sci. Rep.*, 4:6784, 2014.
- [58] D. Foster, C. Kind, P. J. Ackerman, J.-S. Tai, B. M. R. Dennis, and I. I. Smalyukh. Composite skyrmion bags in two-dimensional materials. Preprint: arXiv:1806.02576, 2018.
- [59] A. Vansteenkiste, J. Leliaert, M. Dvornik, M. Helsen, F. Garcia-Sanchez, and B. Van Waeyenberge. The design and verification of MuMax3. *AIP Adv.*, 4:107133, 2014.